JVSTB
JOURNAL OF VACUUM SCIENCE AND TECHNOLOGY B

Three-dimensional micro- and nanostructuring by combination of nanoimprint and x-ray lithography

Massimo Tormen, Filippo Romanato, Matteo Altissimo, Luca Businaro, Patrizio Candeloro et al.

Citation: J. Vac. Sci. Technol. B **22**, 766 (2004); doi: 10.1116/1.1688356
View online: http://dx.doi.org/10.1116/1.1688356
View Table of Contents: http://avspublications.org/resource/1/JVTBD9/v22/i2
Published by the AVS: Science & Technology of Materials, Interfaces, and Processing

Related Articles

From nanocone to nanodisc: Structural transformation of gold nanoarrays via simple mechanical stresses
J. Vac. Sci. Technol. B 30, 06FF10 (2012)

Fabrication of an adhesion-free transparent roll stamp for large area patterning using ultraviolet-type roller nanoimprint lithography
J. Vac. Sci. Technol. B 30, 06FB11 (2012)

Sidewall-angle dependent mold filling of three-dimensional microcavities in thermal nanoimprint lithography
J. Vac. Sci. Technol. B 30, 06FB09 (2012)

Cross-linking control during imprint for hybrid lithography
J. Vac. Sci. Technol. B 30, 06FB08 (2012)

Fabrication of nanodot array mold with 2 Tdot/in.2 for nanoimprint using metallic glass
J. Vac. Sci. Technol. B 30, 061602 (2012)

Additional information on J. Vac. Sci. Technol. B

Journal Homepage: http://avspublications.org/jvstb
Journal Information: http://avspublications.org/jvstb/about/about_the_journal
Top downloads: http://avspublications.org/jvstb/top_20_most_downloaded
Information for Authors: http://avspublications.org/jvstb/authors/information_for_contributors

ADVERTISEMENT

Three-dimensional micro- and nanostructuring by combination of nanoimprint and x-ray lithography

Massimo Tormen,[a] Filippo Romanato, Matteo Altissimo, Luca Businaro, Patrizio Candeloro, and Enzo M. Di Fabrizio
TASC-INFM, Lilit Beamline, S.S. 14-km 163.5, I-34012 Basovizza-Trieste, Italy

(Received 12 November 2003; accepted 29 January 2004; published 17 March 2004)

We present results on a lithographic approach that combines nanoimprint (NIL) and x-ray lithography (XRL) for fabricating unconventional three-dimensional (3D) polymer structures. The use of XRL for structuring a prepatterned resist by NIL gives rise to high-resolution high-aspect-ratio structures whose overall profile is enveloped by the original 3D imprinted profile. The technological potential of this method has been demonstrated by patterning several different types of structures with XRL on an hexagonal array of hemispheres previously obtained by nanoimprinting. © *2004 American Vacuum Society.* [DOI: 10.1116/1.1688356]

I. INTRODUCTION

In the fast run for device miniaturization, microelectronics has relied on planar lithography and layering of essentially two-dimensional structures. Technological advances in micro- and nanoelectromechanical systems,[1] microfluidic devices,[2] micro- or nano-optics (diffractive optics,[3] high efficiency multilevel zone plates,[4] photonic crystals),[5] and innovations in the toolset of biology (microfluidic chips for deoxyribose nucleic acid array)[6] and medicine (microsurgical tools,[7] drug delivery) will require the development of fully three-dimensional (3D) structuring capabilities at the nanometer scale.

Several lithographic techniques have already been explored for 3D structuring at submicron resolution. Electron beam lithography can generate ''gray-scale'' profiles controlling the exposure dose. High resolution x-ray lithography (XRL) can replicate a multilevel mask amplifying the thickness profile[8] and can generate complex 3D structures with multiple exposure at tilted angles.[9] Focused ion beam lithography has shown the capability for direct milling and in the growth of hard materials.[10] Nanoimprint lithography (NIL) can mold 3D profiles.[11] Soft lithography has shown interesting possibilities for fabricating microfluidic network with complex topology[12] or for patterning curved substrate.[13] Interference optical lithography and more recently two-photon lithography[14] are also emerging as 3D patterning techniques.

All lithographies above have their own specificity and potentialities that in many cases are still not completely exploited and cannot cover the entire spectrum of the fabrication needs. However, as we show in the present article, combining two of them allows us to extend the fabrication to a much wider class of micro- and nano-objects that pave the road to device categories. In particular, we demonstrate an approach by consecutive use of NIL and XRL. This allows generating nonconventional 3D structures consisting of high aspect ratio features whose overall envelope is modulated according to the original 3D imprinted profile.

[a]Electronic mail: tormen@tasc.infm.it

II. EXPERIMENTAL METHOD

NIL has 3D structuring capabilities. In order to exploit this aspect a master with continuous 3D profile was fabricated using isotropic etching of a fused silica substrate in order to form an array of hemispherical cavities (Fig. 1 master picture). After the evaporation of a 150 nm Cr layer on a flat substrate of fused silica, an hexagonal array of 4 μm circular holes spaced 20 μm apart were opened in the Cr film by photolithography and chromium wet etching in an ammonium cerium (IV) nitrate (0.6 M) and acetic acid (1 M) aqueous solution. The openings in the chromium layer served as a mask for isotropic wet etching (15 wt % HF in water) of fused silica. This resulted in the formation of $\sim$20 μm diam quasihemispherical cavities. The process of NIL stamp fabrication was completed by stripping the chromium mask. For the imprinting step, a silicon substrate was coated with 6 μm of 950 K poly(methylmetacrylate) (PMMA), and the hot embossing was performed according to standard procedures[15] at a pressure of 20 MPa and a temperature of 210 °C. The separation of the stamp from the imprinted polymer film did not present difficulties even in the absence of any specific treatment of the stamp surface.

After the process of hemispheres imprinting, a set of samples was exposed at the XRL LILIT beam line[16] selecting a spectrum energy window (from 800 to 2.3 keV, peaked at 1.6 keV) that allows the full exposure of the thickest (9 μm) part of the hemispheres. This ensures that the depth of the XRL patterning is completely independent of the local resist thickness. An x-ray mask consisted of a 2 μm thick silicon nitrate membrane with zone plate structures with 500 nm gold in the absorbing regions, corresponding to a transmitted intensity contrast of 15:1 between transparent and absorbing regions. A second x-ray mask consisted of a 2 μm thick Si_3N_4 membranes carrying a variety of gold structures (array of dots, rings, lines, crosses) electroplated to a thickness of 400 nm.

The results we present below have been obtained mounting the masks at two different angles, i.e., $\theta=35°$ and $\theta=0°$ with respect to the x-ray beam. Patterns were exposed on the array of PMMA hemispheres (Fig. 2) with an aerial dose of

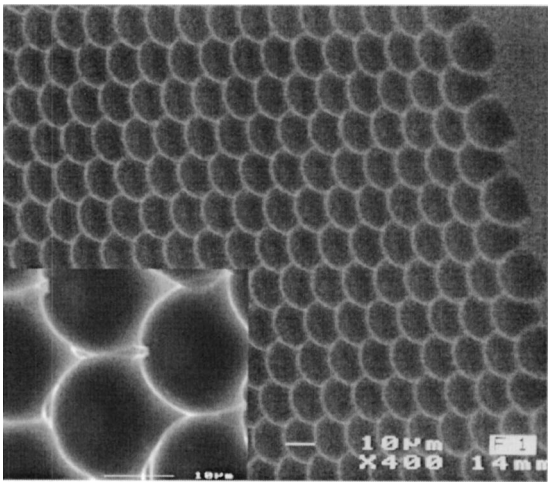

FIG. 1. Array of hemispherical cavities defined on the fused silica master. The bar corresponds to 10 μm.

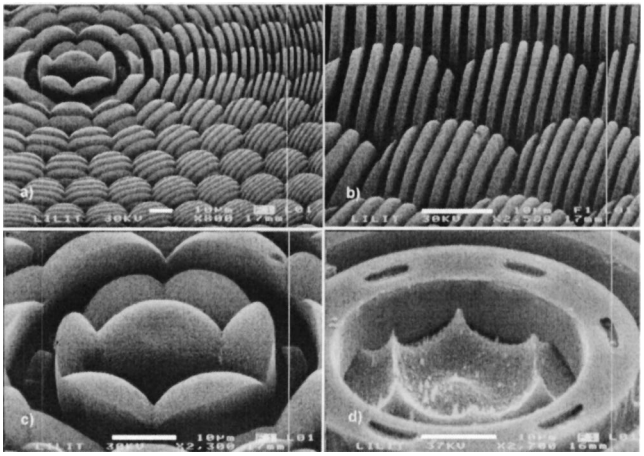

FIG. 3. (a–c) Zone plate structure superimposed to the 3D profile of an array of hemispheres. (d) Inverted 3D structure by nickel electroplating. Bars correspond to 10 μm.

4000 mJ/cm^2 and developed in a solution of metyl-isobutyl chetone and isopropyl alcohol (1:3) for 4 min.

One of the samples that were three-dimensionally structured by NIL/XRL was further processed in order to demonstrate the possibility of generating a master for imprinting or injection molding. The sample was sputter coated with a 40 nm film of palladium–gold. The film was used as base plating for the electrochemical growth of Ni. The electroplating bath was kept at 55 °C and a current density of 150 mA/cm^2 was maintained during the growth up to a deposit thickness of ~100 μm. Finally, in order to release the nickel structure the silicon substrate and the PMMA structured film were dissolved in a 5 M solution of KOH in water.

III. RESULTS

Figure 1 shows an array of PMMA hemispherical holes closely packed in a 20 μm hexagonal lattice at the surface of a fused silica substrate. The imprinted structures in PMMA are homogeneously reproduced on the entire area (~5×5 mm^2) of the stamp that is shown in Fig. 2. With the exception of the edges of the patterned field, where imperfections reproduce defects already present in the master, the surface quality of the imprinted 3D structure appears very high. This results allows us to envisage the possibility of using NIL in the production of optical elements and other devices with stringent fabrication requirements.

The first example of the combined use of NIL and XRL is shown in Fig. 3(a) where a set of concentric circles of a zone plate optic pattern were exposed on an imprinted array of hemispheres. The patterning of the central zone shows a net cutting of the hemispheres [Fig. 3(b)]. The high penetration depth of the x rays makes the lithographic image almost insensitive to the thickness modulation the preexisting structure. At the same time, the high optical contrast of the x-ray mask provides an almost complete radiation absorption in the shadowed areas obtaining a negligible deformation of the unexposed PMMA regions.

The zone plate design represents a severe test pattern because of the progressive reducing period of the concentric rings. In the present case the outermost zone period of 2 μm was successfully reproduced on the hemisphere generating structures with aspect ratios as high as 9 [Fig. 3(c)], i.e., a value that can be considered quite relaxed for x-ray lithography. In this case no specific process to improve the stability of the structures has been used that, on the contrary, could be applied to obtain lithographic resolution on the order of 100 nm and aspect ratio on the order of 10–15.[17]

Crucial for the application of the proposed technique is the possibility of fabricating 3D high resolution masters for nanoimprinting and injection molding suitable for mass production. Figure 3(d) shows the 3D profile of a nickel master obtained inverting the polymer structure by electroplating. All the features of the NIL+XRL pattern are finely reproduced on the master and the cusps at the crossing of three edges are sharp. The origin of a few extra structures in the form of small scale nickel pillars can be traced back to defects in the polymer structure surface. This roughness is likely due to the random dissolution of part of the resist exposed at subthreshold dose, and to the prolonged develop-

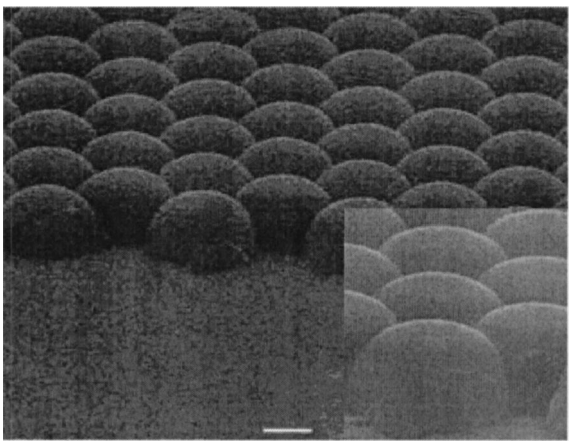

FIG. 2. Hexagonal array of microlenses imprinted in PMMA.

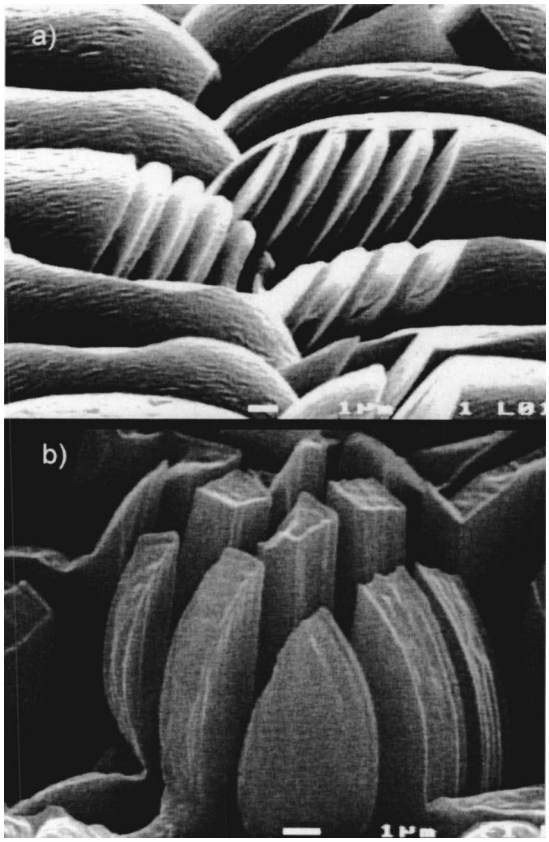

FIG. 4. Examples of trenches formed into curved structures. The cuts are directed at 35° from the normal to the sample substrate. Bars correspond to 1 μm.

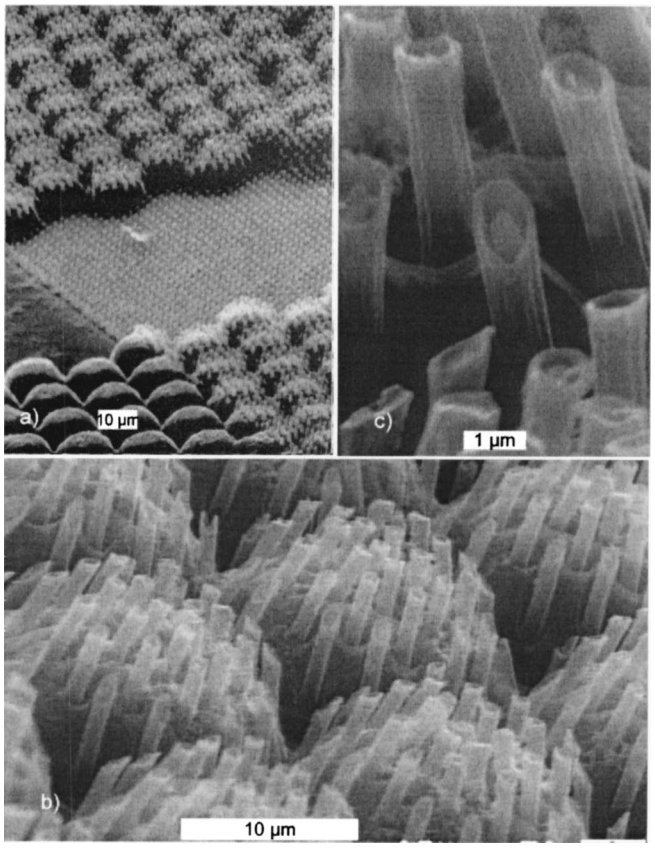

FIG. 5. High spatial frequency features defined by XRL on low spatial frequency structures by NIL.

ing time used to completely develop the fully exposed areas of the pattern. These small defects further testify to the high fidelity of the mastering process, and they can be avoided by slightly optimizing the exposure dose and therefore reducing the developing time.

Net cutting can be performed not only perpendicularly to the substrate surface but also along a tilted direction. Fine tilted structures resulting from the transversal cutting of the hemispheres [Fig. 4(a)] after an exposure of 4000 mJ/cm^2 did not show any structural collapse. The stability of the structures is shown by cutting microsphere slices at several planes [Fig. 4(b)] demonstrating that straight and curved profiles, high aspect ratio, and high resolution can be combined in a single microstructure.

Another interesting technological combination of NIL/XRL is represented by the possibility of creating a superposition of structures with different spatial frequencies. Figure 5(a) shows patterned regions that contain three possible lithographic combination: XRL, NIL, and the overlap of the two. The x-ray generated pattern is formed by a 2 μm pitch square array of high aspect ratio ($>$10) pillars that is also exposed on the 20 μm lattice period of hemispheres. Figure 5(b) clearly shows that the pillar tips are precisely enveloped by the shape of the prepatterned array of hemispheres. This is a complementary approach with respect to the examples shown in Figs. 2 and 3 where the hemispheres were full cut down to the substrate. In this case, we point out that the local profile of the original NIL structure is preserved at the scale of single structures as it can be easily recognized from the slope of the top of the pillars in a closer view image [Fig. 5(c)].

It is worth noting that a full development of the pattern would have completely removed the hemisphere in the exposed area leaving only the standing pillars. On the contrary, we have deliberately developed only partially the patterning to also show that the original shape of the NIL pattern can be progressively dissolved and shrunk almost preserving the original shape. It results in an array of pillars imaginarily stuck on a hemispherical pillow [Fig. 5(b)].

On a closer view further details can be noticed. The pillar tips shows a central column and an external ring that are not present in the original mask, with details at 100 nm scale. At first sight these details could appear quite uncontrolled, resulting from a complex process. This is not the case. The formation of ring structure, corresponding to full dots in the mask, has been already reported as diffraction effects.[18] These are dependent on the spectrum and the coherence of the x-ray source as well as on the resist-mask gap during exposure. We have simulated (TOOLSET code[19]) the operative conditions at which the XRL has been performed experimentally in this work (spectrum peaked at 1.6 keV, 0.83 mrad beam divergence) taking into account the diffraction effects for a mask-resist gap of 10 μm, and the attenuation of the

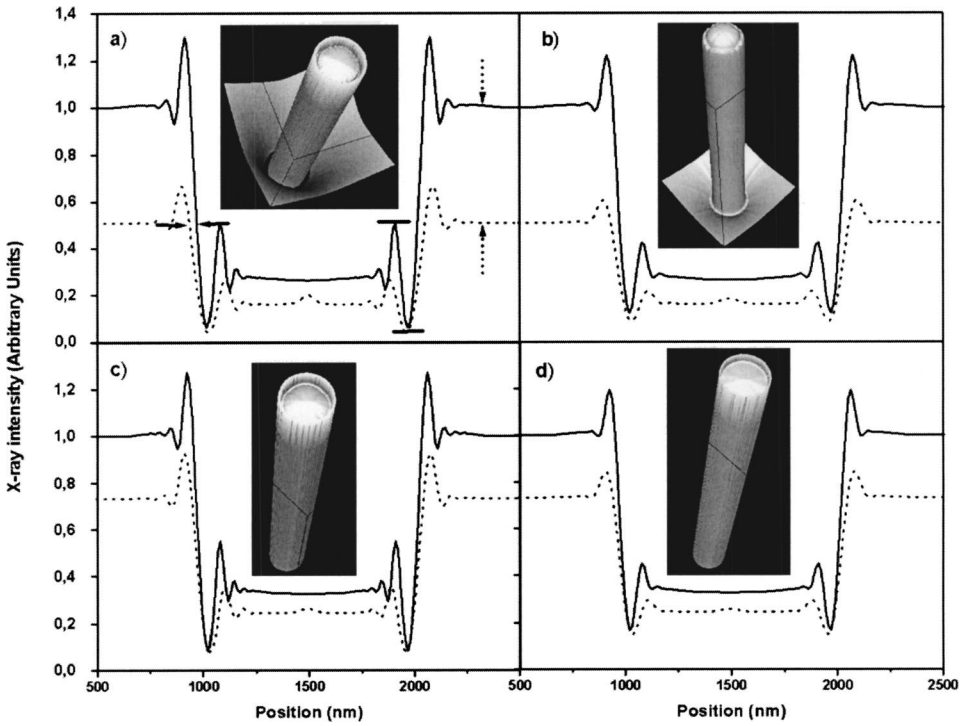

FIG. 6. Simulated dose image curves at the resist surface (continuous lines) and at a depth of 8 μm in the resist (dashed lines) for different exposure conditions: (a) soft spectrum with high spatial coherence; (b) soft spectrum with low spatial coherence; (c) hard spectrum with high spatial coherence; (d) hard spectrum with low spatial coherence (for the quantitative meaning of soft, hard, and low and high spatial coherence see the text). The insets show the 3D simulated structures after development. The simulated structure in (a) is qualitatively in good agreement with the fine structure of the microstructures obtained experimentally [Figs. 5(b) and 5(c)].

x-ray intensity through 9 μm of PMMA resist. The results relative to a 1 μm diam 350 nm thick gold dot as mask absorber are given in terms of lateral dose distribution at different depths in the resist (in the plot are shown only the doses at the resist surface and at the depth of 8 μm). A good qualitative agreement between the experimentally fabricated structures [Fig. 5(a)] and simulations is observed.

Further simulations have been performed using harder energy spectrum (peaked at 2.1 keV) and lower spatial coherence of the x-ray beam (angular blur 1.50 mrad) that are controllable exposure parameters at the LILIT beam line[16,20] [Figs. 6(b)–6(d)]. From the dose intensity curves we extracted three significant parameters. The first parameter is the shift [see arrows in Fig. 6(a)] between the edge positions at the surface and at a depth of 8 μm corresponding to 0.5 transmitted intensity. This shift is 35 nm for (a) and (b) while is 23 nm for (c) and (d), showing that the steepness of the structure walls can be increased using the hard spectrum. The second parameter [see horizontal dashes in Fig. 6(a)] is the amplitude of the ripples normalized to the transmitted intensity in the shadowed region under the absorber (position 1500 nm). In this case the relative amplitudes of the ripples are 1.7, 1.2, 1.4, and 0.9 for (a), (b), (c), and (d), respectively. This indicates that the diffraction effects ''perturbing'' the structures with fine details can be reduced, both reducing the spatial coherence and increasing the hardness of the x-ray beam. The third parameter [see vertical dotted arrows in Fig. 6(a)], which is a measure of the aptitude to expose thick resists, is the ratio between the dose at the depth of 8 μm and at the surface of the resist in the region outside the absorber shadow. In this case we have 0.51 for ''soft'' spectra (a) and (b) and 0.74 for ''hard'' spectra (c) and (d).

IV. DISCUSSION

NIL is a high resolution (sub-10 nm), low cost, high throughput technique that has intrinsically three-dimensional replication potentiality. Due to these characteristics NIL is emerging as a possible mass-production technology in the field of micro- and nanosystems.

The results of Fig. 2 show the capability of NIL to form smooth curved surfaces over a large area. It is evident that a large variety of 3D master profiles can be transferred into a polymer film by NIL. However, principle and practical limitations exist for arbitrary structures. For example, it would be difficult to fabricate arrays of pillars nonperpendicular to the substrate or any structure having overhanging parts. Their presence would make it impossible to separate the mold from the polymer in a nondestructive way. This remark can be translated into a requirement for the stamp surface profile which ensures that after the embossing step no obstruction prevents the removal of the master. The requirement is that the orthogonal projection onto the plane of the stamp substrate of any two nonoverlapping areas at the surface of the 3D stamp must not overlap. A second limitation in the 3D NIL patterning capabilities is related to the aspect ratio of the

structures. Due to stresses produced by shear and tensile forces at the surface of micro- nanostructures during the release of the master, high aspect ratio structures suffer high mechanical stresses and may easily break. At present, the highest aspect ratios that can obtained by NIL are ~3.

Both these NIL limitations do not concern XRL. In this respect, XRL is well known to provide aspect ratios attaining values of ~20 (for structures with μm scale resolution), and resolution that at its present status of development can go below 50 nm. Geometrically, the structures obtainable by XRL can be described as the intersection of the volume shadowed by a two-dimensional pattern defined on a mask with the volume of the resist film. As the two-dimensional pattern of the mask can be projected in arbitrary directions with respect to the resist film, XRL allows us to also define tilted structures. Furthermore, by performing single or multiple exposure at tilted angles it has been possible to build complex three-dimensional structures containing voids and overhanging parts.[9]

Although, Figs. 3(a)–3(c) show the results of a process that could be considered just as a lithography test, it shows that special optical elements containing refractive and diffractive components could be produced. Figure 3(d) shows the negative of the central part of the 3D object obtained by nickel electroplating. This demonstrates that the technique could become particularly suitable for prototyping masters for imprinting and injection molding, thus requiring limited use of a highly expensive technique, while the mass production would be committed to low cost techniques.

All experiments described above have been carried out on PMMA since this can be used both as a resist for x-ray lithography as well as for imprinting. Nevertheless, it would be desirable to widen the class of resists suitable for the NIL/XRL technique, in particular towards negative-type resists. An important aspect which is under investigation is the compatibility of x-ray resists such as the chemically amplified resists (CARs), with the prepatterning process by NIL. Generally, negative tone CARs contain agents, such as photoacid generator and crosslinker, that promote the crosslinking of the polymer upon irradiation and postexposure baking. In this case the chemical species responsible for the crosslinking process usually degrade at the typical temperatures employed in the hot embossing processes. The thermal degradation and the diffusion of the generated acids initiate the thermally assisted cross linking significantly, making the resist unsuitable for further x-ray imaging. We are currently exploring the suitability of positive tone CARs as common resists for NIL and subsequent XRL imaging.

V. CONCLUSION

In conclusion we have shown that performing a step of imprinting into a thermoplastic film and utilizing that prepatterned polymer layer as a resist for x-ray lithography provides a flexible method to fabricate a wide class of complex small-scale 3D structures. The combined method exploits the advantages and overcomes most of the limitations of both imprinting and x-ray lithography. Moreover, the fact that both NIL and XRL are parallel patterning techniques would allow us to upscale the fabrication of complex three dimensional nano- or micro-objects to a mass-production level.

[1]H. G. Craighead, Science **290**, 1535 (2000).
[2]H. Wu, T. W. Odom, D. T. Chiu, and G. M. Whitesides, J. Am. Chem. Soc. **125**, 554 (2003).
[3]P. Ehbets, H. P. Herzig, D. Prongué, and M. T. Gale, Opt. Lett. **17**, 908 (1992).
[4]E. Di Fabrizio, F. Romanato, M. Gentili, S. Cabrini, B. Kaulich, J. Susini, and R. Barrett, Nature (London) **401**, 895 (1999).
[5]Y. A. Vlasov, X. Z. Bo, J. C. Sturm, and D. J. Norris, Nature (London) **414**, 289 (2001).
[6]J. Khandurina and A. Guttman, J. Chromatogr., A **943**, 159 (2002).
[7]M. J. Vasile, R. Nassar, and J. Xie, J. Vac. Sci. Technol. B **16**, 2499 (1998).
[8]P. Mouroulis, F. T. Hartley, D. W. Wilson, and V. E. White, Opt. Express **11**, 270 (2003).
[9]C. Cuisin, A. Chelnokov, J.-M. Lourtioz, D. Decanini, and Y. Chen, Appl. Phys. Lett. **77**, 770 (2000); F. Romanato *et al.*, Microelectron. Eng. **67–68**, 679 (2003).
[10]M. J. Vasile, R. Nassar, and J. Xie, J. Vac. Sci. Technol. B **16**, 2499 (1998).
[11]M. Li, L. Chen, and S. Y. Chou, Appl. Phys. Lett. **78**, 3322 (2001).
[12]J. R. Anderson, D. T. Chiu, R. J. Jackman, O. Cherniavskaya, J. C. McDonald, H. K. Wu, S. H. Whitesides, and G. M. Whitesides, Anal. Chem. **72**, 3158 (2000).
[13]J. A. Rogers, R. J. Jackman, G. M. Whitesides, D. L. Olson, and J. V. Sweedler, Appl. Phys. Lett. **70**, 2464 (1997).
[14]T. Tanaka, H.-B. Sun, and S. Kawata, Appl. Phys. Lett. **80**, 312 (2002).
[15]M. Li, L. Chen, W. Zhang, and S. Y. Chou, Nanotechnology **14**, 33 (2003).
[16]E. Di Fabrizio, A. Nucara, M. Gentili, and R. Cingolani, Rev. Sci. Instrum. **70**, 1605 (1999).
[17]M. Altissimo, F. Romanato, L. Vaccari, L. Businaro, D. Cojoc, B. Kaulich, S. Cabrini, and E. Di Fabrizio, Microelectron. Eng. **61–62**, 173 (2002).
[18]L. Businaro, F. Romanato, P. Candeloro, E. Di Fabrizio, M. Patrini, M. Galli, C. Andreani, A. Passaseo, and M. De Vittorio, J. Vac. Sci. Technol. B **21**, 748 (2003).
[19]M. Khan, L. Mohammad, J. Xiao, L. Ocola, and F. Cerrina, J. Vac. Sci. Technol. B **12**, 3930 (1994).
[20]F. Romanato, E. Di Fabrizio, L. Vaccari, M. Altissimo, D. Cojoc, L. Businaro, and S. Cabrini, Microelectron. Eng. **57–58**, 101 (2001).